Published in final edited form as:
Neurogastroenterol Motil. 2012 December ; 24(12): . doi:10.1111/nmo.12035.

Full-field optical coherence microscopy is a novel technique for imaging enteric ganglia in the gastrointestinal tract

E. CORON[*,†,‡,§,1], **E. AUKSORIUS**[*,1], **A. PIERETTI**[¶,1], **M. M. MAHÉ**[†,‡,§], **L. LIU**[*], **C. STEIGER**[¶], **Y. BROMBERG**[*], **B. BOUMA**[*,**], **G. TEARNEY**[*,**,††,2], **M. NEUNLIST**[†,‡,§,2], and **A. M. GOLDSTEIN**[¶,2]

[*]Wellman Center for Photomedicine, Massachusetts General Hospital and Harvard Medical School, Boston, MA, USA

[†]INSERM UMR 913, Nantes, France

[‡]Digestive Diseases Institute, University Hospital of Nantes, Nantes, France

[§]Faculty of Medicine, University of Nantes, Nantes, France

[¶]Department of Pediatric Surgery, Massachusetts General Hospital and Harvard Medical School, Boston, MA, USA

[**]Harvard-MIT Division of Health Sciences and Technology, Boston, MA, USA

[††]Department of Pathology, Massachusetts General Hospital and Harvard Medical School, Boston, MA USA

Abstract

Background—Noninvasive methods are needed to improve the diagnosis of enteric neuropathies. Full-field optical coherence microscopy (FFOCM) is a novel optical microscopy modality that can acquire 1 μm resolution images of tissue. The objective of this research was to demonstrate FFOCM imaging for the characterization of the enteric nervous system (ENS).

Methods—Normal mice and EdnrB$^{-/-}$ mice, a model of Hirschsprung's disease (HD), were imaged in three-dimensions ex vivo using FFOCM through the entire thickness and length of the gut. Quantitative analysis of myenteric ganglia was performed on FFOCM images obtained from whole-mount tissues and compared with immunohistochemistry imaged by confocal microscopy.

Address for Correspondence Allan M. Goldstein, Massachusetts General Hospital, Warren, 1153, Boston, MA 02114, USA. Tel: 617 726 0270; fax: 617 726 2167; agoldstein@partners.org.

[1]Co-first authors.
[2]Co-senior authors.

DISCLOSURE
None.

CONTRIBUTORS
EC worked on all phases of the study, including imaging, IHC, data analysis, and manuscript preparation. EA was involved in tissue preparation, imaging, co registration, and specimen analysis and contributed to manuscript revision. AP performed mouse husbandry, mouse and human tissue preparation, IHC, and data analysis. MMM performed IHC and data/statistical analyses. LL, CS, and YB were involved in tissue preparation, imaging, and specimen analysis. YB contributed to manuscript revision. BB contributed to study design and image/data analysis. GT contributed to study design, image analysis, and manuscript revision. MN contributed to study design, image and data analysis, and manuscript preparation. AMG, principal investigator, was involved in all phases of the work, including initial study design, data analysis and interpretation, and manuscript preparation.

SUPPORTING INFORMATION
Additional Supporting Information may be found in the online version of this article:
Please note: Wiley-Blackwell are not responsible for the content or functionality of any supporting materials supplied by the authors. Any queries (other than missing material) should be directed to the corresponding author for the article.

Key Results—Full-field optical coherence microscopy enabled visualization of the full thickness gut wall from serosa to mucosa. Images of the myenteric plexus were successfully acquired from the stomach, duodenum, colon, and rectum. Quantification of ganglionic neuronal counts on FFOCM images revealed strong interobserver agreement and identical values to those obtained by immunofluorescence microscopy. In EdnrB$^{-/-}$ mice, FFOCM analysis revealed a significant decrease in ganglia density along the colorectum and a significantly lower density of ganglia in all colorectal segments compared with normal mice.

Conclusions & Inferences—Full-field optical coherence microscopy enables optical microscopic imaging of the ENS within the bowel wall along the entire intestine. FFOCM is able to differentiate ganglionic from aganglionic colon in a mouse model of HD, and can provide quantitative assessment of ganglionic density. With further refinements that enable bowel wall imaging in vivo, this technology has the potential to revolutionize the characterization of the ENS and the diagnosis of enteric neuropathies.

Keywords

enteric nervous system; enteric neuropathies; Hirschsprung's disease; optical coherence microscopy; optical coherence tomography

INTRODUCTION

Enteric neuropathies are associated with many disorders of the gastrointestinal (GI) tract, primarily with those conditions that manifest with severe intestinal dysmotility affecting portions of, or the entire, GI tract.[1,2] A range of morphologic abnormalities of enteric neurons have been described in congenital and acquired GI disorders, including aganglionosis in Hirschsprung's disease (HD),[3] inflammatory enteric neuropathies,[4,5] and even neurodegenerative diseases such as Parkinson's disease.[6]

The diagnosis of enteric neuropathies is currently limited by the need for intestinal biopsies, the absence of guidelines for neuropathologic assessment, and the lack of normative data, especially regarding normal neuronal number and density along the GI tract. Histopathologic methods are time-consuming and can give variable results depending on tissue handling and processing, variability in immunohistochemical staining, and the inadequacy of tissue sections for morphometric evaluations. In addition, discrepancies are common between counts obtained from different observers.[7] Furthermore, biopsies are often reserved for the most severe cases, thereby limiting available histopathologic data.[8,9] To improve understanding of enteric neuropathies, develop better approaches to their diagnosis and treatment, and allow novel nosologic classifications, improved tools for examining normal and abnormal enteric nervous system (ENS) morphology are needed.

Major progress toward meeting these needs has recently been achieved by developing a technical procedure that allows the analysis of the ENS on whole mounts of submucosal plexus.[10] Indeed, using standard biopsies obtained endoscopically, loss of submucosal neurons was identified in Parkinson's disease[6] and imaging of calcium activity was performed in human enteric submucosal neurons.[11] However, one major drawback is that standard biopsies only allow assessment of the submucosal plexus. To date, accessing the myenteric plexus requires full-thickness biopsies using surgical approaches, which are invasive and therefore limited to the most severe cases. Alternative approaches using endoscopic full-thickness biopsies, as recently performed in large animal models,[12–15] might be used in the future provided that safety can be demonstrated. However, these techniques are invasive, limited to examination of small samples of bowel, and are prone to sampling error. In addition, standard pathological approaches are also associated with delays in tissue processing. Therefore, real-time noninvasive mapping of full-thickness segments of the GI

tract and, in particular, identification of ENS structures such as ganglia or even single neurons would represent a major step forward in the characterization of enteric neuropathies.

Recent developments of optical methods such as optical coherence tomography (OCT) allow depth-resolved images of tissue architecture with an axial resolution of 10–15 μm and a transverse resolution of 15–25 μm without the need for the administration of contrast agents. Endoscopic OCT was successfully used to characterize mucosal structures in pathologies such as Barrett's esophagus, biliary or pancreatic cancers or inflammatory bowel diseases in the colon.[16–20] However, one major drawback of OCT is its low resolution when compared with confocal endomicroscopy, prohibiting the visualization of cells or neuronal process, which is vital in assessing the ENS. A hybrid technique, termed optical coherence microscopy addresses this limitation by combining the high axial sectioning capabilities of OCT with the high transverse resolution of confocal microscopy, achieving cellular resolution imaging in the transverse or en face plane. In particular, full-field optical coherence microscopy (FFOCM), initially developed by Dubois et al.[21,22], has been used to image healthy and cancerous human colonic mucosa[23,24] at the cellular level ex vivo. The goal of this study was to demonstrate the ability of FFOCM to image the ENS and to perform precise quantification of ganglionic and neuronal density.

METHODS

Animal model and tissues

Experiments were approved by the Institutional Animal Care and Use Committee at Massachusetts General Hospital. The mouse strain used was the Ednrb$^{tm1Ywa/J}$ targeted mutation on a hybrid C57BL/6J-129Sv background (JAX stock no. 003295). The Ednrb$^{tm1Ywa/J}$ mutation segregates in an autosomal recessive manner. Homozygous pups (Ednrb$^{-/-}$) were identified by their white coat color. Genotyping was performed using a polymerase chain reaction-based assay to distinguish wildtype (Ednrb$^{+/+}$) from heterozygous (Ednrb$^{+/-}$) mice. A total of four EdnrB$^{-/-}$ mice and three wild-type littermates were studied. Mice were euthanized with CO_2 asphyxiation on postnatal day 21 (P21). Laparotomy was performed and the entire colorectum removed. The colon was opened longitudinally along the antimesenteric axis, stretched on a Sylgard plate, and fixed with 4% paraformaldehyde prior to imaging. To assess the ability of FFOCM to image human myenteric ganglia, surgically resected cecum was obtained under an IRB approved protocol from a 19-year-old female who underwent ileo-cecal resection for Crohn's disease. The tissue was rinsed, stretched, and pinned onto an agarose plate. The mucosa, submucosa, and circular muscle layers were removed and the tissue fixed with 4% paraformaldehyde.

FFOCM

Full-field optical coherence microscopy is based on conventional wide-field light microscopy with an auxiliary reference arm that together forms a Linnik interferometer.[21] The reference arm is utilized to select a specific imaging depth by interfering the reference light with the image of the specimen. The interference will occur only between photons that travel the same path-length in the sample and in the reference arm. Hence, for a fixed path length of the reference arm, the interference optically selects an *en face* image from a specific depth in the sample.[21] A water immersion objective lens (20× W, NA = 0.5, Olympus America Inc., Chelmsford, MA, USA) was used in each of the sample and reference arms, yielding a transverse resolution of 0.75 μm. Xenon arc lamp (Oriel 6263; Newport Corporation, Irvine, CA, USA) at 600 ± 100 nm was used to provide an optical sectioning thickness or axial resolution of 0.8 μm in tissue. We estimated axial resolution by measuring the 'full width at half maximum' of the plane response function of the FFOCM system and transverse resolution using the first derivative of the measured edge response

function. These methods for resolution measurement are standard in our field.[21,25] Images with 512 × 512 pixels were obtained with a CMOS camera (1M150, Dalsa, Waterloo, Ontario, Canada or MV-D1024E-160-CL-12, PhotonFocus, Lachen, Switzerland) with an acquisition time of approximately 2 s per *en face* image. Three-dimensional datasets were obtained using a motorized stage (Picomotor 8302, New Focus, Santa Clara, CA, USA) to depth scan the sample in steps of 0.25 μm. Image processing and analysis were performed using Image J Software v1.42q (National Institutes of Health, Bethesda, MD, USA).

Full-field optical coherence microscopy imaging was performed over 350 μm depth on fresh or fixed samples of stomach, duodenum, and colorectum from wild-type mice. Imaging was conducted from the serosal side of the tissue, allowing visualization of serosa, longitudinal muscle, myenteric ganglia, circular muscle, submucosa, and mucosa in the stomach (Movie S1), duodenum (Movie S2), and colon (Movie S3).

Immunohistochemistry

Tissue was permeabilized for 5 h in PBS/NaN_3 containing 1% Triton X-100 (Sigma, St-Quentin Fallavier, France), 0.05% saponin (Quijilla bark; Sigma), and 10% donkey serum (Millipore, Billerica, MA, USA). Tissue then was rinsed and blocked for 3 h with PBS and 2% donkey serum. The mouse anti-HuC/D (Invitrogen, Courtaboeuf, France) was labeled with a Cyanine 3 (anti-HuC/D-Cy3) protein labelling kit (GE Healthcare, Velizy, France). Whole-mount immunohistochemistry (IHC) was performed in two steps: (i) incubation with conjugated mouse anti-HuC/D-Cy3 (1 : 200; 400 mg mL^{-1}) for 12 h and (ii) incubation with rabbit anti-PGP9.5 (1 : 2000; Ultraclone, Wellow, UK) for 12 h followed by incubation for 3 h with donkey antirabbit IgG conjugated to Alexa Fluor 488 (Invitrogen). After final washes, the tissue was laid flat on a microscope slide and mounted in a resinous fluorescence mounting medium (Gold Prolong Medium; Invitrogen).

For immunohistochemical studies on human tissue, after blocking with 10% goat serum and 1% BSA, anti-Tuj1 antibody (Covance, Princeton, NJ, USA) was applied overnight, followed by addition of secondary antibody (Alexafluor 594, anti-mouse IgG) for 1 h.

Acquisition settings for confocal imaging

Confocal imaging was performed with a Nikon A1R confocal microscope equipped with 20× Plan-Apochromat objective (Nikon, Champigny sur Marne, France). Images were acquired at 1024 × 1024 (X/Y) with a z-axis increment of 3 μm. Image processing and analysis was performed using Image J Software v1.42q (National Institutes of Health).

Co-registration with FFOCM and fluorescence microscopy

A conventional wide-field fluorescence microscope was incorporated into the FFOCM system by adding appropriate excitation (short pass 512 nm) and emission (band pass 540/50 nm) filters and a separate sensitive CCD camera (Cascade II:512, Photometrics, Tucson, AZ, USA), as described.[26] The system can be switched between FFOCM and fluorescence microscopy, thus allowing acquisition of FFOCM and fluorescence images from the same area on a micrometre scale. As conventional wide-field fluorescence microscopy cannot reject out-of-focus light, we implemented structured illumination fluorescence microscopy to enable optical sectioning by inserting a grid in the illumination path of the microscope.[26,27]

Statistical analysis

Data are expressed as mean ± SD. Experimental data were compared using two-way ANOVA followed by Bonferonni post-test. Interobserver agreement on the presence or

absence of ganglia and neuronal counts was evaluated by three independent examiners. For each pair of examiners, correspondence findings were compared using kappa analysis. Agreement among examiners was compared statistically using a Bland-Altman analysis.[28]

RESULTS

FFOCM imaging of the gut wall

Cross-sectional reconstruction of FFOCM images in mice demonstrated the capability of this technology to enable full-thickness visualization of the gut wall, with identification of the myenteric ganglia (Fig. 1A). In addition, individual en face images were examined at each layer of the gut wall and myenteric ganglia could be clearly identified between the longitudinal and circular muscle layers in the gastric fundus (Fig. 1B), duodenum (Fig. 1C), and colon (Fig. 1D). Full-field optical coherence microscopy also provided high-resolution imaging of submucosal blood vessels (Fig. 1E) and mucosal crypts (Fig. 1F).

FFOCM imaging of the myenteric plexus

We next determined the ability of FFOCM to morphologically and quantitatively assess the myenteric plexus in the colorectum from wild-type mice. Co-localized FFCOM and optically sectioned immunofluorescence recording of Hu- and PGP9.5-labeled tissue was performed. Immunofluorescence identified enteric neuronal cell bodies and interganglionic nerve fibers in the myenteric plexus (Fig. 2A). Co-localized recording of FFOCM and fluorescence images showed strikingly similar morphology, with optically dense structures containing multiple, round cell bodies as well as projecting fibers (Fig. 2B). Overlay of the two images confirms that these round structures identified by FFOCM represent enteric ganglion cells (Fig. 2C). To extend these results, the number of neuronal cell bodies per μm^2 of ganglion was compared quantitatively between FFOCM and IHC at multiple sites along the colorectum. For FFOCM, large, round structures contained within a ganglion were counted as neurons. A minimum of two neurons adjacent to each other was required to constitute a ganglion, consistent with a published definition of enteric ganglia.[29] The calculated density of neuronal cells was similar using the two methods (Fig. 2D).

Interobserver agreement analysis

To evaluate interobserver agreement on the presence or absence of myenteric ganglia by FFOCM imaging, three independent examiners (A,B,C) determined whether myenteric ganglia were present in four sets of images, with each set comprising nine images from wild-type colon and 12 images from mutant colon. Kappa analysis was used to statistically measure the observed agreement relative to agreement expected by chance. The results, summarized in Table 1, show a high rate of concordance, with kappa values ranging from 0.77 to 1.00. To further quantify the degree of interobserver agreement, we compared the number of neurons counted in each of 28 FFOCM images by the three different examiners. This statistical comparison was performed using Bland-Altman plots, in which the difference in the number of neurons counted by each pair of examiners is plotted against the mean number of ganglia. A total of six plots were generated, each comprising a pair-wise comparison of two of the three examiners. The variation was uniform across the data range, indicating no evidence of bias in relation to the number of neurons present. Furthermore, the random scatter indicated the absence of any systematic error. In all six plots, only three data points exceeded the limits of agreement, defined as two standard deviations from the mean.

FFOCM imaging of the myenteric plexus network in a model of HD

Full-field optical coherence microscopy was used to perform a morphological analysis of the myenteric plexus in a mouse model of HD, the $EdnrB^{-/-}$ mutant, which is characterized by

distal colorectal aganglionosis. A stack of 100 ± 40 images was acquired at multiple sites along the colon and rectum from the serosal side, focusing on the interface between longitudinal and circular muscles, where the myenteric plexus is located. Full-field optical coherence microscopy images in wild-type mice consistently revealed the presence of ganglionic structures in 92%, 75%, and 83% of images in the proximal colon, mid colon, and rectum, respectively. In contrast, in Erdnb$^{-/-}$ mutant mice, the presence of ganglionic structures was observed in only 56%, 50%, and 13% of images in the proximal colon, mid colon, and rectum, respectively. Similar morphologic differences were shown by FFOCM and confocal IHC, with abundant myenteric ganglia throughout the colorectum in normal mice (Figs 3A–F), while EdnrB$^{-/-}$ mice displayed mild hypoganglionosis in the proximal colon and severe hypoganglionosis/aganglionosis distally (Figs 4A–F).

To quantitatively validate the morphologic observations made in Figs 3 and 4, the number of myenteric ganglia per μm^2 was determined by FFOCM at four distinct sites in the proximal colon, mid colon, and rectum of EdnrB$^{-/-}$ mice and wild-type mice (Fig. 5). These results confirm a statistically significant difference in the density of ganglia present along the rostrocaudal length of the mutant colorectum, when compared with the homogeneous distribution in normal mice.

FFOCM imaging of myenteric ganglia in human colon

In order to establish the potential clinical utility of FFOCM in humans, samples of human cecum were analyzed following removal of the mucosa, submucosa, and circular muscle. *En face* imaging of whole-mount tissue from the mucosal side allowed identification of ganglionic structures. Co-registration of samples with FFOCM and immunofluorescence following Tuj-1 labeling confirmed that FFOCM accurately identified structures corresponding to enteric ganglia (Fig. 6).

DISCUSSION

Our study demonstrates the ability of FFOCM to perform real-time optical imaging of the myenteric plexus in the GI tract of mouse and human. In addition, FFOCM was able to identify and quantify the extent of aganglionosis and hypoganglionosis in a mouse model of HD with excellent interobserver agreement. FFOCM is based on the technology behind OCT, an emerging technique for imaging of biological samples with micrometer-scale resolution. In recent years, higher resolution FFOCM has been explored as a novel alternative approach to OCT, which is based on white-light interference microscopic imaging. In contrast to conventional OCT, the entire imaging field is illuminated with a simple halogen/xenon arc lamp and there is no scanning of a tightly focused beam. Tomographic images in the *en face* orientation are obtained by combining interferometric images acquired in parallel using a CCD/CMOS digital camera. Due to the ultrashort coherence length of the illumination source, the axial resolution is 0.8 μm, higher than that of conventional OCT and similar to the resolution of a microscope with a high power objective.[21]

While FFOCM has been successfully used to image brain and sciatic nerve, cancer cell lines, GI tissues, vocal fold, and other tissue,[23,24,30–32] no data exist on the ability of FFOCM to image the ENS. Our results expand the applications of FFOCM to include assessment of the ENS, showing the ability of FFOCM to provide morphologic and quantitative information regarding myenteric ganglia, including ganglionic area and neuronal counts. We found that the assessment of neuronal density by FFOCM was similar to that obtained using standard IHC with Hu antibody. As Hu is a highly reliable pan-neuronal marker for the ENS,[33] this finding indicates that all neurons can be identified with FFOCM. Importantly, this was further highlighted by co-localized image acquisition using

FFOCM and fluorescence microscopy built on the same optical set-up, which enabled direct image comparison from the same area and represents an important technological advance.[26] One of the major advantages of FFOCM is that it allows real-time optical sectioning of full-thickness segments of intestine with high resolution, both in fresh and fixed tissue. FFOCM provides full-thickness images of the gut wall in mice, including blood vessels, muscle fibers, connective tissue, and mucosal crypts. In addition, FFOCM provides en face images similar to those obtained with whole-mount staining of the ENS. En face imaging is critically important to obtain quantitative normative data, such as neuronal cell density, as it provides visualization of the whole myenteric plexus. In contrast, standard cross-sectional histology provides images of only thin sections, leading to potentially important sampling bias. Another advantage of FFOCM is that it requires no contrast agent or fluorescent labeling to identify ganglia and neuronal cell bodies. However, FFOCM is limited by its use of interferometry, which does not allow fluorescence imaging of the ENS, a useful tool for defining the precise neurochemical phenotype of the ENS, nor does it allow functional assessment by the use of voltage-sensitive or calcium-sensitive fluorophores.[34,35]

Our study identified several other limitations of the technique that need to be addressed. To obtain maximal image quality of the myenteric plexus, we needed to image samples from the serosal, rather than mucosal, side. While this approach is amenable to laparoscopic imaging, mucosal imaging will need to be improved to allow endoscopic evaluation of the ENS. Factors that influence imaging quality in FFOCM are speed, image contrast, and depth. Currently FFOCM images at about one frame per second, so any motion of the specimen can cause artifacts. Investigators are working on increasing FFOCM speed to facilitate robust in vivo imaging. Image contrast in FFOCM is related to the difference in reflectance between distinct tissue types. While FFOCM can obtain high quality images of tissue, sources of contrast in FFOCM in human tissues merit significant future study. Penetration depth of FFOCM is different for different tissue types. In our case, we found that penetration through the serosa to the mucosa was possible, especially in mouse intestine. However, with thicker human tissues, we had difficulty penetrating to the myenteric plexus. Full-field optical coherence microscopy at longer wavelengths[36] should mitigate this problem and may allow for robust imaging of the myenteric plexus in humans. The current FFOCM system is a bench top model and is therefore limited for in vivo and *in situ* use. Further research aimed at developing a FFOCM-based endoscopic or laparoscopic system is required. This is certainly feasible as early prototype FFOCM devices that are compatible with laparoscopy[37] and flexible endoscopy have been developed.[25,38]

We were able to successfully apply FFOCM imaging to mice with null mutations of the EdnrB gene as a proof of principle to test the ability of FFOCM to identify and evaluate colorectal aganglionosis. EdnrB$^{-/-}$ mice represent an established model of HD, with mice having a variable length of colorectal aganglionosis.[39] FFOCM was consistently able to identify the aganglionic distal segment in these mice. Furthermore, we observed a significant decrease in ganglion density in the proximal colon of the EdnrB$^{-/-}$ mice when compared with controls. Similar changes have previously been reported in the same model[40,41] as well as in other models of HD.[42] The high degree of heterogeneity in ganglion density in the proximal mutant colon reflects the wide variability in both length of aganglionic colon in this model as well as the variable degree of hypoganglionosis present proximally.[39] From a clinical perspective, accurate delineation of the aganglionic, normoganglionic, and intervening hypoganglionic regions is critically important for determining the appropriate level for surgical transection,[40] which is currently carried out based on intra-operative frozen section evaluation of H&E-stained sections. Furthermore, pathologists often examine >100 H&E-stained sections to establish or exclude the initial diagnosis of HD.[40] Real-time imaging of the ENS would facilitate the diagnosis and surgical management of this condition. In addition, for the pathologic evaluation of HD and other

neuroenteric disorders, interobserver variability is a major limitation of current histopathologic techniques.[7,29] We tested interobserver variability in interpretation of FFOCM images by performing kappa analyses and Bland-Altman statistics. Analysis of neuronal density by different investigators showed a highly statistically significant interobserver concordance among blinded evaluators who analyzed the same FFOCM images. An important limitation to our study is that we imaged only one human specimen, as a proof of concept, and the feasibility of FFOCM imaging of myenteric neurons in humans still has to be evaluated in a larger number of patients.

In conclusion, FFOCM has the potential to provide reliable morphologic and quantitative assessment of the ENS in fresh or fixed gut specimen in mice and human. However, further developments are needed to perform such analyses in vivo. With further refinements, these techniques may ultimately enable live imaging of the ENS along any portion of the GI tract. This capability would be a major step forward toward improving the diagnosis of enteric neuropathies.

Supplementary Material

Refer to Web version on PubMed Central for supplementary material.

Acknowledgments

Confocal microscopy was performed in the Cellular and Tissular Imaging Core Facility of Nantes University (MicroPICell). We are grateful to Elk Halpern for expert assistance with statistical analyses and to Joseph Gardecki for technical assistance.

FUNDING

This work was supported by NIH R01HL076398, R01HL093717, R01CA103769, and R01DK091923 to GT. EC was supported by the University Hospital of Nantes and by a grant from the SanTdige Foundation. MM was supported by a grant from Nantes Metropole. AMG was supported by R01DK080914.

Abbreviations

ENS	enteric nervous system
FFOCM	full-field optical coherence microscopy
GI	gastrointestinal
HD	Hirschsprung’s disease
IHC	immunohistochemistry
OCT	optical coherence tomography

References

1. Knowles CH, De Giorgio R, Kapur RP, et al. Gastrointestinal neuromuscular pathology: guidelines for histological techniques and reporting on behalf of the Gastro 2009 International Working Group. Acta Neuropathol. 2009; 118:271–301. [PubMed: 19360428]
2. Knowles CH, De Giorgio R, Kapur RP, et al. The London Classification of gastrointestinal neuromuscular pathology: report on behalf of the Gastro 2009 International Working Group. Gut. 2010; 59:882–7. [PubMed: 20581236]
3. Kapur RP. Neuropathology of paediatric chronic intestinal pseudoobstruction and related animal models. J Pathol. 2001; 194:277–88. [PubMed: 11439358]
4. De Giorgio R, Guerrini S, Barbara G, et al. Inflammatory neuropathies of the enteric nervous system. Gastroenterology. 2004; 126:1872–83. [PubMed: 15188182]

5. Coron E, Flamant M, Aubert P, et al. Characterisation of early mucosal and neuronal lesions following *Shigella flexneri* infection in human colon. PLoS ONE. 2009; 4:e4713. [PubMed: 19274103]
6. Lebouvier T, Neunlist M, des Varannes SB, et al. Colonic biopsies to assess the neuropathology of Parkinson's disease and its relationship with symptoms. PLoS ONE. 2010; 5:e12728. [PubMed: 20856865]
7. Swaminathan M, Kapur RP. Counting myenteric ganglion cells in histologic sections: an empirical approach. Hum Pathol. 2010; 41:1097–108. [PubMed: 20346481]
8. Wedel T, Spiegler J, Soellner S, et al. Enteric nerves and interstitial cells of Cajal are altered in patients with slow-transit constipation and megacolon. Gastroenterology. 2002; 123:1459–67. [PubMed: 12404220]
9. Tomita R, Howard ER. Clinical studies on anorectal myectomy for chronically constipated patients with outlet obstruction in childhood. Hepatogastroenterology. 2008; 55:1600–5. [PubMed: 19102350]
10. Lebouvier T, Coron E, Chaumette T, et al. Routine colonic biopsies as a new tool to study the enteric nervous system in living patients. Neurogastroenterol Motil. 2010; 22:E11–4. [PubMed: 19650774]
11. Cirillo C, Tack JF, Vanden Berghe P. Measuring nerve activity in routine human intestinal biopsies. Gastroenterology. 2011; 140:S4–5.
12. Neunlist M, Coquenlorge S, Aubert P, et al. Colonic endoscopic full-thickness biopsies: from the neuropathological analysis of the myenteric plexus to the functional study of neuromuscular transmission. Gastrointest Endosc. 2011; 73:1029–34. [PubMed: 21521570]
13. Rajan E, Gostout CJ, Lurken MS, et al. Endoscopic "no hole" full-thickness biopsy of the stomach to detect myenteric ganglia. Gastrointest En-dosc. 2008; 68:301–7.
14. Raju GS, Malhotra A, Ahmed I. Colonoscopic full-thickness resection of the colon in a porcine model as a prelude to endoscopic surgery of difficult colon polyps: a novel technique. Gastrointest Endosc. 2009; 70:159–65. [PubMed: 19559838]
15. von Renteln D, Schmidt A, Vassiliou MC, Rudolph H-U, Caca K. Endoscopic full-thickness resection and defect closure in the colon. Gastrointest Endosc. 2010; 71:1267–73. [PubMed: 20598252]
16. Evans JA, Poneros JM, Bouma BE, et al. Optical coherence tomography to identify intramucosal carcinoma and high-grade dysplasia in Barrett's esophagus. Clin Gastroenterol Hepatol. 2006; 4:38–43. [PubMed: 16431303]
17. Evans JA, Bouma BE, Bressner J, et al. Identifying intestinal metaplasia at the squamocolumnar junction by using optical coherence tomography. Gastrointest Endosc. 2007; 65:50–6. [PubMed: 17137858]
18. Testoni PA, Mangiavillano B. Optical coherence tomography in detection of dysplasia and cancer of the gastrointestinal tract and bilio-pancreatic ductal system. World J Gastroenterol. 2008; 14:6444–52. [PubMed: 19030194]
19. Familiari L, Strangio G, Consolo P, et al. Optical coherence tomography evaluation of ulcerative colitis: the patterns and the comparison with histology. Am J Gastroenterol. 2006; 101:2833–40. [PubMed: 17227526]
20. Shen B, Zuccaro G Jr, Gramlich TL, et al. In vivo colonoscopic optical coherence tomography for transmural inflammation in inflammatory bowel disease. Clin Gastroenterol Hepatol. 2004; 2:1080–7. [PubMed: 15625653]
21. Dubois A, Vabre L, Boccara AC, Beaurepaire E. High-resolution full-field optical coherence tomography with a Linnik microscope. Appl Opt. 2002; 41:805–12. [PubMed: 11993929]
22. Dubois A, Grieve K, Moneron G, Lecaque R, Vabre L, Boccara C. Ultrahigh-resolution full-field optical coherence tomography. Appl Opt. 2004; 43:2874–83. [PubMed: 15143811]
23. Choi WJ, Jeon DI, Ahn S-G, Yoon J-H, Kim S, Lee BH. Full-field optical coherence microscopy for identifying live cancer cells by quantitative measurement of refractive index distribution. Opt Express. 2010; 18:23285–95. [PubMed: 21164669]
24. Choi ES, Choi WJ, Ryu SY, et al. Feasibility of full-field optical coherence microscopy in ultra-structural imaging of human colon tissues. J Korean Phys Soc. 2010; 57:79–83.

25. Oh WY, Bouma BE, Iftimia N, Yelin R, Tearney GJ. Spectrally-modulated full-field optical coherence microscopy for ultrahigh-resolution endoscopic imaging. Opt Express. 2006; 14:8675–84. [PubMed: 19529248]
26. Auksorius E, Bromberg Y, Motiejuenaite R, et al. Dual-modality fluorescence and full-field optical coherence microscopy for biomedical imaging applications. Biomed Opt Express. 2012; 3:661–6. [PubMed: 22435110]
27. Neil MA, Juskaitis R, Wilson T. Method of obtaining optical sectioning by using structured light in a conventional microscope. Opt Lett. 1997; 22:1905–7. [PubMed: 18188403]
28. Bland JM, Altman DG. Statistical methods for assessing agreement between two methods of clinical measurement. Lancet. 1986; 1:307–10. [PubMed: 2868172]
29. Knowles CH, Veress B, Kapur RP, et al. Quantitation of cellular components of the enteric nervous system in the normal human gastrointestinal tract – report on behalf of the Gastro 2009 International Working Group. Neurogastroenterol Motil. 2011; 23:115–24. [PubMed: 21175997]
30. Ben Arous J, Binding J, Leger JF, et al. Single myelin fiber imaging in living rodents without labeling by deep optical coherence microscopy. J Bio-med Opt. 2011; 16:116012.
31. Boudoux C, Leuin SC, Oh WY, et al. Optical microscopy of the pediatric vocal fold. Arch Otolaryngol Head Neck Surg. 2009; 135:53–64. [PubMed: 19153308]
32. Jain M, Shukla N, Manzoor M, Nadolny S, Mukherjee S. Modified full-field optical coherence tomography: a novel tool for rapid histology of tissues. J Pathol Inform. 2011; 2:28. [PubMed: 21773059]
33. Phillips RJ, Hargrave SL, Rhodes BS, Zopf DA, Powley TL. Quantification of neurons in the myenteric plexus: an evaluation of putative pan-neuronal markers. J Neurosci Methods. 2004; 133:99–107. [PubMed: 14757350]
34. Cirillo C, Tack J, Vanden Berghe P. Nerve activity recordings in routine human intestinal biopsies. Gut. 2012 Mar 2. [Epub ahead of print].
35. Hosoda K, Hammer RE, Richardson JA, et al. Targeted and natural (piebald-lethal) mutations of endothelinB receptor gene produce megacolon associated with spotted coat color in mice. Cell. 1994; 79:1267–76. [PubMed: 8001159]
36. Oh WY, Bouma BE, Iftimia N, Yun SH, Yelin R, Tearney GJ. Ultrahighresolution full-field optical coherence microscopy using InGaAs camera. Opt Express. 2006; 14:726–35. [PubMed: 19503391]
37. Latrive A, Boccara AC. In vivo and in situ cellular imaging full-field optical coherence tomography with a rigid endoscopic probe. Biomed Opt Express. 2011; 2:2897–904. [PubMed: 22025991]
38. Ford HD, Tatam RP. Fibre imaging bundles for full-field optical coherence tomography. Meas Sci Technol. 2007; 18:2949–57.
39. Kapur RP. Can we stop looking? Immunohistochemistry and the diagnosis of Hirschsprung disease. Am J Clin Pathol. 2006; 126:9–12. [PubMed: 16753604]
40. Coventry S, Yost C, Palmiter RD, Kapur RP. Migration of ganglion cell precursors in the ileoceca of normal and lethal spotted embryos, a murine model for Hirschsprung disease. Lab Invest. 1994; 71:82–93. [PubMed: 8041122]
41. Miyahara K, Kato Y, Koga H, et al. Abnormal enteric innervation identified without histopathologic staining in aganglionic colorectum from a mouse model of Hirschsprung's disease. J Pediatr Surg. 2010; 45:2403–7. [PubMed: 21129555]
42. Uesaka T, Nagashimada M, Yonemura S, Enomoto H. Diminished Ret expression compromises neuronal survival in the colon and causes intestinal aganglionosis in mice. J Clin Invest. 2008; 118:1890–8. [PubMed: 18414682]

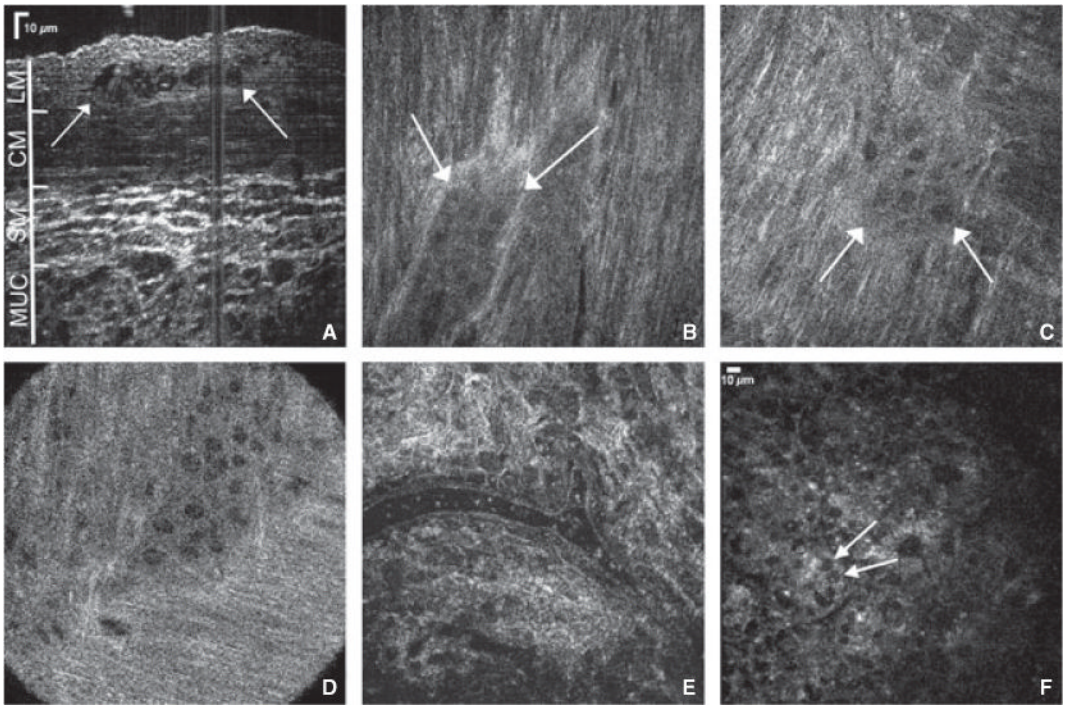

Figure 1.

Full-field optical coherence microscopy provides high resolution full-thickness imaging of gut wall. Cross-sectional reconstruction of stacked planar images obtained from the serosal side of the mouse colon reveals full-thickness colonic wall structures (A, arrows depict myenteric ganglion). Myenteric ganglia are visualized in gastric fundus (B), duodenum (C), and proximal colon (D). A colonic submucosal blood vessel containing erythrocytes is seen (E), as are crypts in the colonic mucosa (F, arrows mark goblet cells in the colon epithelium). LM, longitudinal muscle; CM, circular muscle; SM, submucosa; MUC, mucosa.

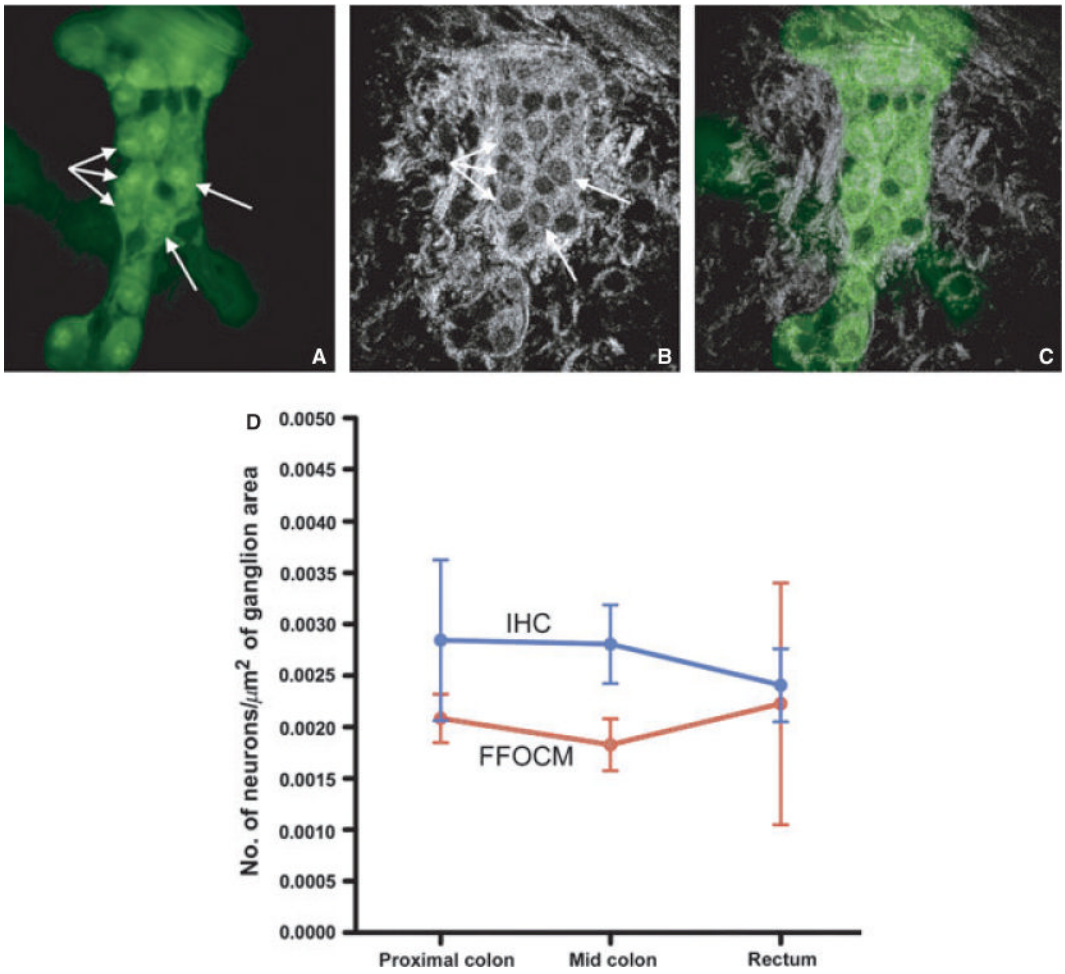

Figure 2.

Full-field optical coherence microscopy (FFOCM) and fluorescence microscopy yield similar images of enteric ganglia. Whole-mount immunohistochemistry (IHC) using PGP9.5 and Hu antibodies were performed of myenteric ganglia in the colon (A). Hu-immunoreactive neuronal cells bodies (A, arrows) and interganglionic PGP9.5-labeled nerve fibers are seen. Both stains are green in the picture as a single excitation/emission filter pair was used, resulting in the excitation as well as detection of fluorescence of both fluorophores. Colocalized recording of FFOCM images (imaged from the serosal side) (B) demonstrates highly similar ganglion morphology, as confirmed by image overlay of the two techniques (C). To compare FFOCM and fluorescence IHC quantitatively, the number of ganglion cells in proximal colon, mid colon, and rectum from a wild-type mouse were counted using each method and the results compared. No statistically significant differences were found (D).

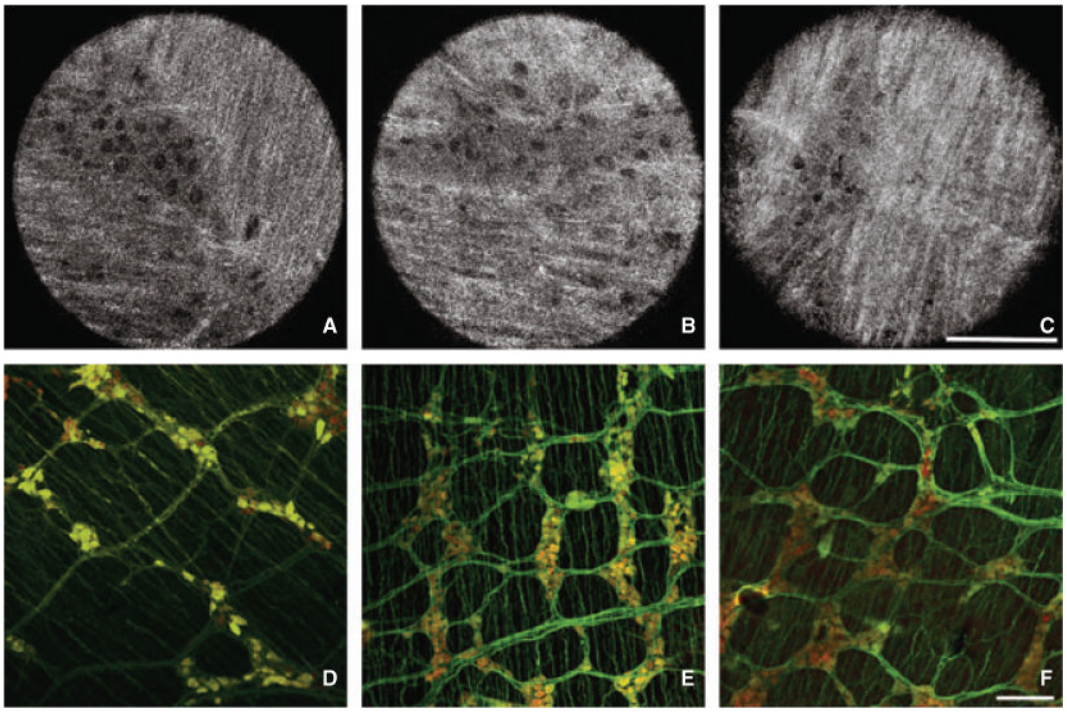

Figure 3.

Morphologic assessment of enteric ganglia in normal mice by Full-field optical coherence microscopy (FFOCM) and whole-mount immunohistochemistry (IHC). Representative images from FFOCM (imaged from the serosal side) and PGP9.5 (green)/Hu (red) whole-mount IHC were obtained from the proximal colon (A,D), mid colon (B,E), and rectum (C,F). The colorectum displays normal-appearing enteric ganglia consisting of groups of neuronal cell bodies connected by interganglionic nerve fibers. FFOCM images are representative 'real' single images. Confocal microcopy images are shown with larger field of view to provide representative images of a large gut segment. Scale bars in C and F are 100 μm.

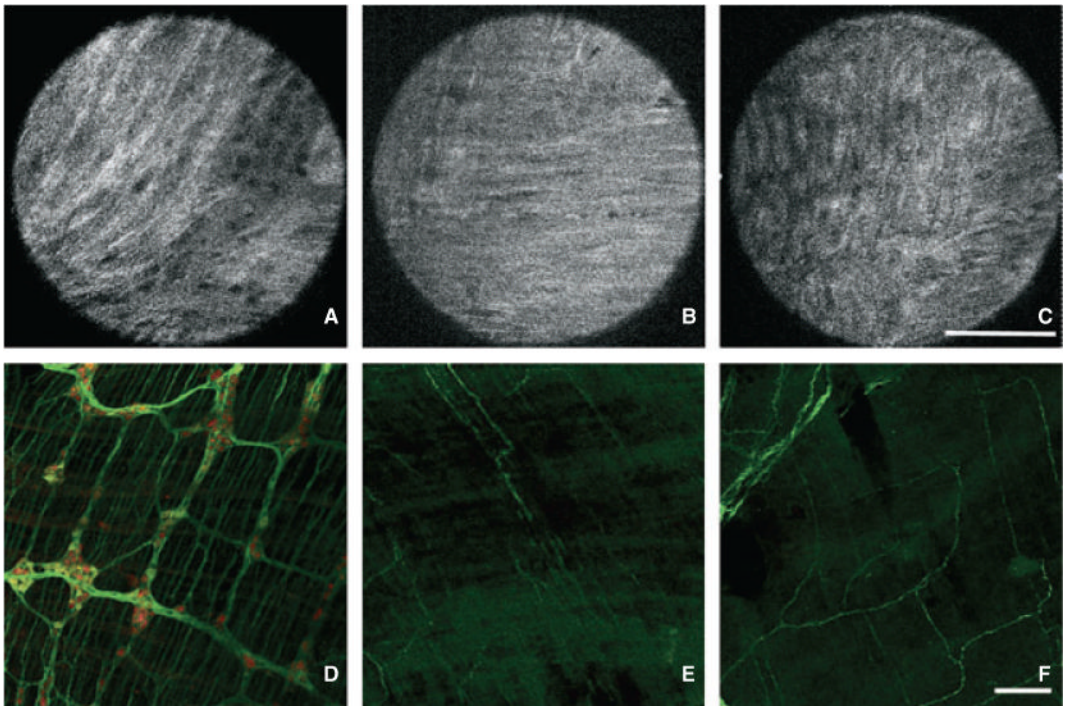

Figure 4.

Morphologic assessment of enteric ganglia in Hirschsprung's mice by Full-field optical coherence microscopy (FFOCM) and whole-mount immunohistochemistry (IHC). Representative images from FFOCM (imaged from the serosal side) and PGP9.5 (green)/Hu (red) whole-mount IHC were obtained from the proximal colon (A,D), mid colon (B,E), and rectum (C,F) of EdnrB$^{-/-}$ mice. The proximal colon is hypoganglionic while the distal segments have no visible ganglia in the images shown. FFOCM images are representative 'real' single images. Confocal microcopy images are shown with larger field of view in order to provide representative images of a large gut segment. Scale bars in C and F are 100 μm.

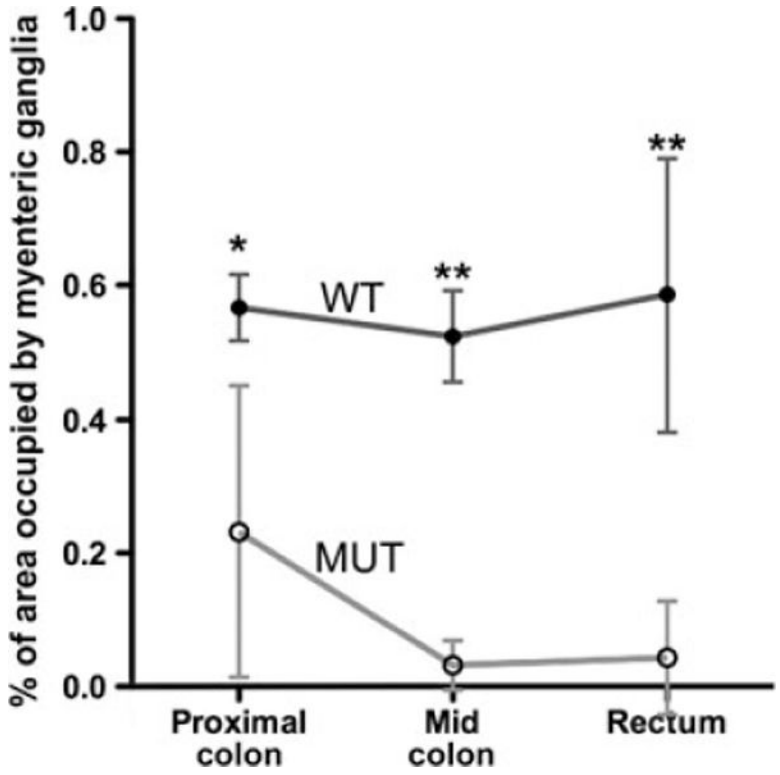

Figure 5.

Quantitative comparison of colorectal myenteric ganglion density by Full-field optical coherence microscopy (FFOCM) in normal and EdnrB$^{-/-}$ mice. Wild-type (WT; $n = 4$) and mutant (MUT; $n = 5$) mice were examined by FFOCM at four different sites in the proximal colon, mid colon, and rectum. Myenteric ganglion density remained consistent along the length of the normal colorectum, while EdnrB$^{-/-}$ colon displayed significant hypoganglionosis, with ganglion density decreasing distally. *$P < 0.05$, **$P < 0.0001$.

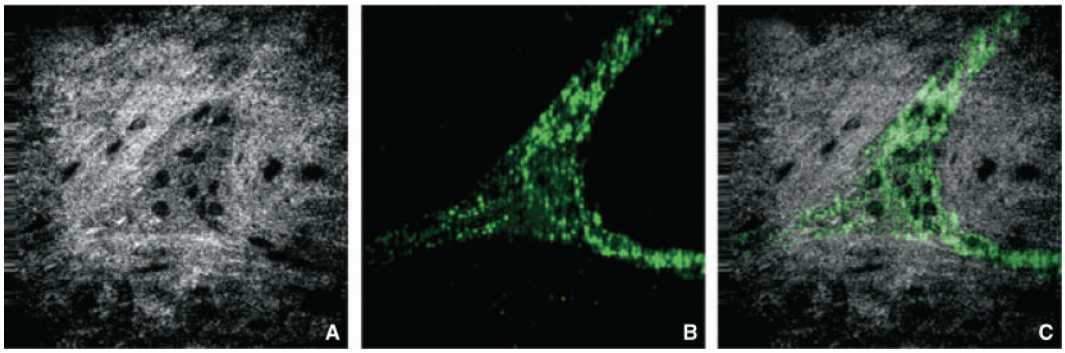

Figure 6.
Full-field optical coherence microscopy (FFOCM) and fluorescence co-registration of human myenteric ganglia. Myenteric ganglion in human cecum was imaged by FFOCM (A) and immunofluorescence following labeling with Tuj1 antibody (B), which labels neuronal processes and not cell bodies. Image overlay (C) of images acquired with the two techniques from the same site.

Table 1

Interobserver concordance for assessing presence of myenteric ganglia

Image set	A *vs* B	A *vs* C	B *vs* C
1	0.90 (0.70–1.00)	0.90 (0.70–1.00)	1.00 (1.00–1.00)
2	0.90 (0.70–1.00)	0.90 (0.71–1.00)	0.80 (0.54–1.00)
3	0.77 (0.47–1.00)	0.77 (0.47–1.00)	0.79 (0.50–1.00)
4	0.90 (0.70–1.00)	0.90 (0.70–1.00)	0.80 (0.53–1.00)

Results are expressed as kappa values (95% confidence intervals).